VIP Cathode Materials Very Important Paper

Deutsche Ausgabe: DOI: 10.1002/ange.201506408
Internationale Ausgabe: DOI: 10.1002/anie.201506408

Nanoscale Surface Modification of Lithium-Rich Layered-Oxide Composite Cathodes for Suppressing Voltage Fade

Fenghua Zheng, Chenghao Yang, Xunhui Xiong, Jiawen Xiong, Renzong Hu, Yu Chen, and Meilin Liu**

Abstract: *Lithium-rich layered oxides are promising cathode materials for lithium-ion batteries and exhibit a high reversible capacity exceeding 250 mAh g^{-1}. However, voltage fade is the major problem that needs to be overcome before they can find practical applications. Here, $Li_{1.2}Mn_{0.54}Ni_{0.13}Co_{0.13}O_2$ (LLMO) oxides are subjected to nanoscale $LiFePO_4$ (LFP) surface modification. The resulting materials combine the advantages of both bulk doping and surface coating as the LLMO crystal structure is stabilized through cationic doping, and the LLMO cathode materials are protected from corrosion induced by organic electrolytes. An LLMO cathode modified with 5 wt% LFP (LLMO–LFP5) demonstrated suppressed voltage fade and a discharge capacity of 282.8 mAh g^{-1} at 0.1 C with a capacity retention of 98.1% after 120 cycles. Moreover, the nanoscale LFP layers incorporated into the LLMO surfaces can effectively maintain the lithium-ion and charge transport channels, and the LLMO–LFP5 cathode demonstrated an excellent rate capacity.*

Lithium-ion batteries (LIBs) are considered to be a promising energy-storage technology and are widely used in purely electric vehicles (PEVs) and hybrid electric vehicles (HEVs).[1,2] However, the energy density of state-of-the-art LIBs is limited, which directly affects the driving range of the vehicle between charges and is one of the main problems keeping them from practical applications. Generally, the cathode has been regarded as the capacity-determining component of a LIB.[3] Among the developed cathode materials, Li-rich layered oxides, $x\,Li_2MnO_3{\cdot}(1-x)LiMO_2$ (M = Ni, Co, and Mn; $0.2 \le x \le 0.7$) have attracted significant interest owing to their high reversible capacity, which exceeds 250 mAh g^{-1} in the 2.0–4.8 V voltage range.[4,5]

Typically, Li-rich layered oxides are composed of monoclinic Li_2MnO_3 ($C2m$) and hexagonal a-$NaFeO_2$-structured $LiMO_2$ ($R\bar{3}m$), and can also be written as $Li_{1+x}M_{1-x}O_2$. The crystal structure of lithium-rich layered Li_2MO_3 can be related to that of layered $LiMO_2$, with the excess lithium ions occupying transition metal (TM) ion sites in the TM layer (Supporting Information, Figure S1 B). Therefore, the Li_2MO_3 component plays a vital role in storing the excess lithium and securing the high voltage and specific capacity. However, a gradual decrease of the average charge–discharge voltage has been observed for lithium-rich layered oxides when they were cycled above 4.5 V, which is referred to as "voltage fade".[6–9] The continuous voltage fade results in a dramatic decrease of the cathode energy density. The migration of TM ions from the TM layer to the lithium layer, which is accompanied by local phase transformations from hexagonal layered to cubic spinel structures (Figure S2) caused by frequent (de)intercalation processes, during cycling above 4.5 V is thought to be the main reason for the voltage fade.[10,11] Meanwhile, lithium-rich layered oxides have been found to be unstable in highly lithiated/delithiated states with charge/discharge voltages above 4.5 V, leading to exothermic reactions with electrolytes and accelerated voltage/capacity fade.[9]

The cationic doping of $Li_{1+x}M_{1-x}O_2$ with Al,[12] Ti,[13] Zn,[14] Cr,[15] Y,[16] or Mg[17] is an effective approach that has been extensively studied for stabilizing the crystal structure and minimizing the voltage fade. Meanwhile, coating the surfaces of lithium-rich layered oxides with metal fluorides (AlF_3),[18] metal oxides (Al_2O_3, MgO, ZrO_2, and ZnO),[19–22] or metal phosphates ($AlPO_4$ and $CoPO_4$),[23,24] is widely used to prevent them from etching by the electrolytes. Both surface coating and doping are novel methods for modifying the structure and improving the cycling stability of lithium-rich layered oxides. However, as most of the cationic dopants and surface-coating layers are electrochemically inactive during the charge/discharge processes, the advanced structural and cycling stability comes at the cost of reducing the specific capacity and energy density of the cathode. Moreover, as most of the surface-coating layers have low electronic or lithium-ion conductivity, they will block the ion and charge transport channels on the surface of lithium-rich layered oxides and reduce their rate capacities. Recently, Nanda et al. reported the use of a nanometer-thick lithium-conducting solid electrolyte (lithium phosphorus oxynitride, LiPON) as a coating for lithium-rich layered oxides, $Li_{1.2}Mn_{0.525}Ni_{0.175}Co_{0.1}O_2$; the resulting cathode exhibited excellent rate performance and capacity retention.[7,25]

[*] F. Zheng, Prof. C. Yang, Dr. X. Xiong, J. Xiong, Prof. M. Liu
New Energy Research Institute
College of Environment and Energy
South China University of Technology
382 Waihuan Road, Guangzhou Higher Education Mega Center,
Guangzhou 510006 (P. R. China)
E-mail: esyangc@scut.edu.cn
Prof. R. Hu
School of Materials Science and Engineering
South China University of Technology
Guangzhou 510640 (P. R. China)
Dr. Y. Chen, Prof. M. Liu
School of Materials Science & Engineering
Georgia Institute of Technology
Atlanta, GA 30332-0245 (USA)
E-mail: meilin.liu@mse.gatech.edu

Supporting information for this article is available on the WWW under http://dx.doi.org/10.1002/anie.201506408.

Herein, we describe the incorporation of a nanoscale electrochemically active $LiFePO_4$ (LFP) into the surface of lithium-rich layered oxides, $Li_{1.2}Mn_{0.54}Ni_{0.13}Co_{0.13}O_2$ (LLMO), by a facile sol–gel method. As illustrated in Figure S3, a thin layer of LFP was homogenously coated on the LLMO surface, and can serve to protect the LLMO cathodes from the corrosion induced by organic electrolytes. Various amounts of LFP were doped into LLMO surface, which led to the formation of a thin layer of a LLMO–LFP solid solution (transition layer), which can effectively stabilize the LLMO crystal structure. The morphology and structure of pristine and surface-modified LLMO were then studied to understand their effects on the LLMO cycling stability.

Cyclic voltammetry (CV) measurements from 2.0 to 4.8 V at a scan rate of 0.1 $mV\,s^{-1}$ were performed to investigate the kinetic behavior of pristine LLMO and two LFP-surface-modified LLMO samples (3 or 5 wt% LFP: LLMO–LFP3 and LLMO–LFP5, respectively). In the first CV cycle of LLMO (Figure S5A), two pairs of anodic peaks were observed at 4.08 and 4.62 V in the charge process. The anodic peak at 4.08 V corresponds to lithium de-intercalation from the LLMO accompanied by the oxidation of Ni^{2+} to Ni^{4+} and Co^{3+} to Co^{4+}, while the anodic peak at 4.7 V corresponds to the Mn^{4+} activation process and further lithium de-intercalation from LLMO.[26,27] However, the anodic peak at 4.7 V, which is associated with the irreversible removal of Li_2O from the Li_2MnO_3 component during the charge process, disappeared in following cycles. Owing to the activation of the Li_2MnO_3 component by its decomposition to Li_2O and MnO_2, an anodic peak at 3.4 V became apparent, which was ascribed to the oxidation/reduction of Mn^{3+}/Mn^{4+}. Moreover, a gradual increase in the intensity of the intercalation peak below 3.0 V, which corresponds to the reduction of Mn^{4+} in the spinel phase, was clearly detected, suggesting the increased formation of a spinel phase within LLMO.[9,28] However, the intercalation peak below 3.0 V was not observed during cycling with LLMO–LFP3 and LLMO–LFP5 (Figure S5B,C), and transformations of the local phase from a layered into a spinel structure were greatly mitigated in surface-modified LLMOs. Furthermore, LLMO–LFP3 and LLMO–LFP5 have specific capacities of 296.5 and 288.4 $mAh\,g^{-1}$ with irreversible capacities (ICs) of 19.1% and 19.0%, respectively; these values are much higher than those for pristine LLMO (257.3 $mAh\,g^{-1}$, 25.5% IC; Figure S5D).

SEM/TEM images of pristine LLMO show that as-prepared LLMO is well-crystallized with a particle size of approximately 300 nm (Figure 1A,C). A HRTEM image of LLMO (Figure 1E) reveals the distance between lattice fringes to be 0.47 nm, which corresponds to the (003) plane of hexagonal layered LLMO. Surface-modified LLMO–LFP5 particles have a morphology similar to that of LLMO, but with a contrast between the core and shell regions indicating the formation of LLMO–LFP core–shell structures (Figure 1B,D). The core–shell structures have an average core diameter of approximately 300 nm and a shell thickness of about 7 nm. HRTEM analysis demonstrates that the inner core and the external shell have lattice spacings of 0.47 and 0.35 nm, which can be indexed to the (003) plane of LLMO and the (201) plane of LFP, respectively (Figure 2F,G). An atomic-resolution image of an LLMO–LFP5 sample together with an atomic model of the hexagonal $R\bar{3}m$ unit cell viewed along the $<100>$ direction is shown in Figure 1G. The crystal structure of LLMO–LFP5 corresponds to an a-$NaFeO_2$-type structured LLMO, with a stacking order of Li/O/TM(Li)/O. However, a TEM image of LLMO–LFP5 (Figure 1F) reveals that a thin layer with lattice distortions coexists between the crystalline lattices of LLMO and LFP, suggesting a slight altering of the local environment by surface modification.

Cross-sectional SEM images and the corresponding EDX results are shown in Figure 2 and Figure S6. Fe was mainly located in the shell and in the transition layers. The shell and transition layers were rich in P, but a certain amount (ca.

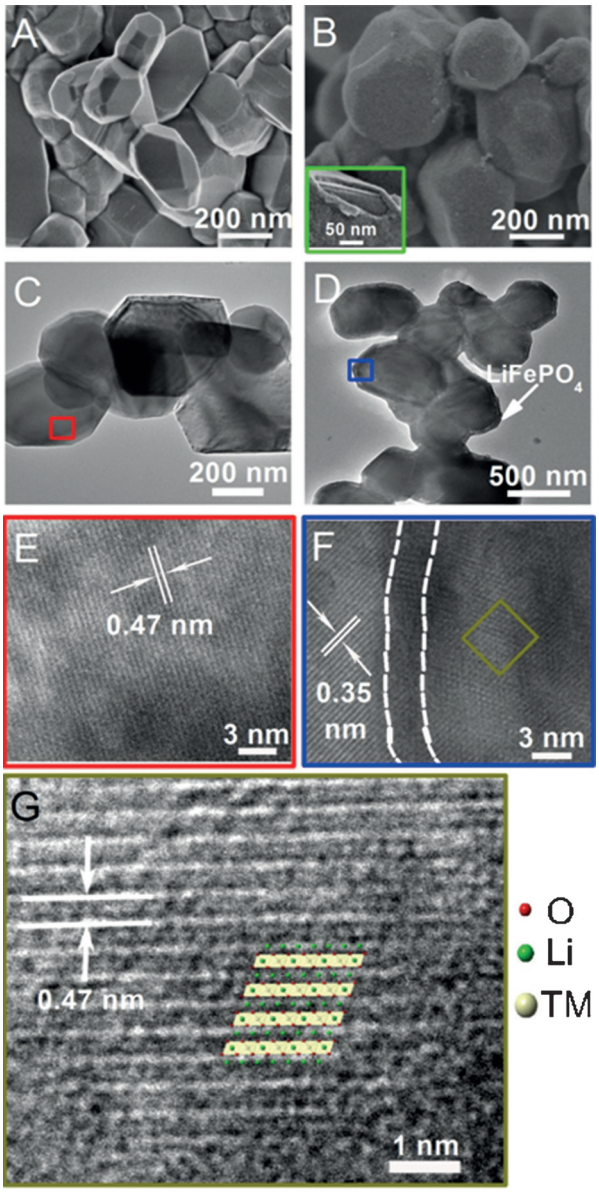

Figure 1. SEM, TEM, and HRTEM images of LLMO (A, C, and E) and LLMO–LFP3 (B, D, and F). The inset in (B) shows the LLMO–LFP core–shell structure. G) Atomic-resolution image of LLMO–LFP5 and schematic illustration of a-$NaFeO_2$-type structured LLMO with the same scale.

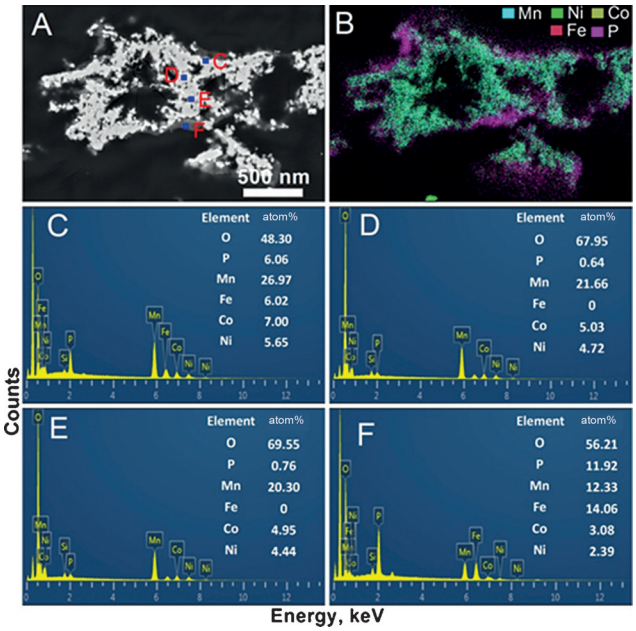

Figure 2. A) Cross-sectional SEM image of LLMO–LFP5. B) Corresponding EDS elemental mapping of O, P, Mn, Fe, Co, and Ni. C–F) EDX microanalysis of selected areas in (A).

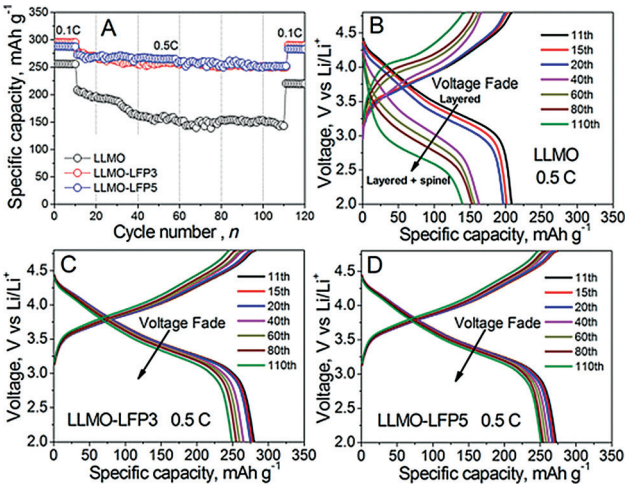

Figure 3. A) Cycling performance and B–D) charge–discharge curves of batteries based on LLMO, LLMO–LFP3, and LLMO–LFP5 cathode materials at 0.5 C between 2.0 and 4.8 V (vs. Li/Li^+) at room temperature.

1 atom%) of P was also detected in the bulk LLMO core. EDX elemental mapping (Figure 2B) shows a Fe- and P-rich shell and a core rich in Mn, Ni, and Co, further confirming the formation of core–shell-structured LLMO–LFP particles. The relatively weak contrast between the LFP shell and the LLMO core indicates the diffusion of Fe/P and Mn/Ni/Co between the core and shell phases and the formation of transition layers, which is due to the concentration gradient during high-temperature calcination. As described in the Supporting Information, citric acid was used as a chelating agent, and the mixture was heated to 80°C for five hours to obtain a transparent gel to prepare the LFP-surface-modified precursors. This process can also be considered as an acid treatment; the H^+/L^+ exchange reaction and de-intercalation of Li_2O from the layered structure are the two main processes that would happen on LLMO surface.[29,30] After high-temperature calcination, Fe ions would occupy the Li^+ sites in the transition layer of the layered structure on citric acid treated LLMO surfaces, which can effectively restrain the migration of TM ions during cycling. Correspondingly, PO_4^{3-} polyanions would occupy the cubic close-packed oxygen sites (Figure S7). The replacement of the strongly electronegative, cubic O^{2-} anions by large tetrahedral PO_4^{3-} polyanions can alter the local environment in the layered structure and has a great effect on the TM cation ordering.[31] As the migration of TM ions can trigger the transformation of the local phase from a layered into a spinel structure and as voltage fade is sensitive to phase transformations, the incorporation of LFP into LLMO surfaces can effectively suppress Mn dissolution (Table S2), stabilize the layered structure, and mitigate the voltage fade. Moreover, the nanometer-thick electrochemically active LFP layers that were homogenously coated onto LLMO surfaces have high electronic and lithium-ion conductivities, and benefit from lithium-ion and charge transport on the LLMO surface.

The cycling performance and selected charge–discharge profiles of LLMO, LLMO–LFP3, and LLMO–LFP5 are shown in Figure 3. LLMO shows a stable capacity at 0.1 C, but the specific capacity degraded substantially when the material was cycled below 0.5 C (Figure 3A). Meanwhile, the corresponding discharge profile of LLMO below 0.5 C showed obvious voltage fade with increased cycling numbers (Figure 3B), and the average discharge potential decreased from 3.49 V for the 11th cycle to 2.74 V for the 110th cycle upon cycling below 0.5 C. On the contrary, the LLMO–LFP3 and LLMO–LFP5 cathodes exhibited excellent rate capabilities and cycling performances after 120 cycles, and the voltage fade was observed to be negligible during the cycling (Figure 3C,D). In particular, LLMO–LFP5 demonstrated an excellent cycling stability, with a first discharge capacity of 282.8 mAh g^{-1} at 0.1 C and a high specific capacity of 249.8 mAh g^{-1} at 0.5 C after 110 cycles, and it even maintained a specific capacity of 277.4 mAh g^{-1} when the sample was returned back to the 0.1 C rate. This value is comparable to that reported for LiPON-coated $Li_{1.2}Mn_{0.525}Ni_{0.175}Co_{0.1}O_2$ (with a specific capacity of 275 mAh g^{-1} after 300 cycles) by Nanda and co-workers.[25]

Moreover, compared to LLMO, LFP-surface-modified LLMO samples exhibit an enhanced rate capacity. As indicated in Figure S8, LLMO–LFP5 has specific discharge capacities of 282.8, 269.1, 201.3, and 125.3 mAh g^{-1} at 0.1, 0.5, 1, and 5 C, respectively. After 120 cycles, LLMO–LFP5 still displayed high specific discharge capacities of 277.4, 249.8, 177.6, and 90.8 mAh g^{-1} at 0.1, 0.5, 1, and 5 C, respectively. The rate capacities of LFP-surface-modified LLMO cathode materials are much higher than those of LLMO materials doped with electrochemically inactive cations or coated with other materials,[12–24] which is ascribed to the thin LFP shell promoting lithium-ion and charge transfer on the LLMO surface. However, the specific capacities of LLMO–LFP5 at

1 and 5 C are lower than those of $Li_{1.2}Mn_{0.525}Ni_{0.175}Co_{0.1}O_2$ coated with a thin layer of LiPON reported by Nanda et al.,[25] indicating that the rate performance of LLMO–LFP5 can be further improved by optimizing its microstructure, for example, by reducing the LFP shell thickness or coating the LFP shell with a thin layer of carbon.[32]

SEM and TEM images of LLMO and LLMO–LFP5 samples after extensive cycling are shown in Figure 4. The surface of pristine LLMO was found to be severely corroded (Figure 4 A, C), and local amorphous domains have formed and coexist with the layered structure (Figure 4 E). The selected-area electron diffraction (SEAD) pattern of LLMO after cycling is shown in Figure 4 G, clearly showing the diffraction patterns from the (0006) and $(10\bar{1}0)$ planes of LLMO, and the (220) and (440) planes of the spinel phase. In contrast, the morphology and microstructure of LLMO–LFP5 after cycling were similar to those of as-prepared LLMP–LFP5 (Figure 4 B, D, F). The SAED pattern of LLMO–LFP5 after cycling along the zone axis is shown in Figure 4 G; a parallelogram reflection composed of four neighboring bright spots can be clearly observed; meanwhile, an orthogonal reflection consisting of three dark spots can also be seen in the parallelogram. The existence of these three dark spots indicates the presence of Li_2MnO_3-like domains and corresponds to the ordering of lithium ions with TM ions in the TM layers as interpreted in Figure S5 G.[10] However, these three dark spots nearly disappeared after cycling, demonstrating that the Li_2MnO_3 had almost been consumed and transformed into hexagonal a-$NaFeO_2$-structured layered oxides.

In conclusion, nanoscale lithium-rich layered oxides, $Li_{1.2}Mn_{0.54}Ni_{0.13}Co_{0.13}O_2$ (LLMO), were modified with a $LiFePO_4$ (LFP) surface by a sol–gel method. The nanoscale LFP surface-coating layer effectively prevented side reactions between the LLMO cathode and organic electrolytes, and promotes ion and charge transfer on the LLMO surface. Meanwhile, the incorporation of LFP into the LLMO surface layer can effectively restrain the migration of TM ions and stabilize the crystal structure of local phases during high-voltage cycling. These results suggest that the functional surface modification of lithium-rich layered oxides, for example, with LFP, is an effective approach to protect the electrode from being etched by organic electrolytes, suppress voltage fade, and improve the long-term cycling stability.

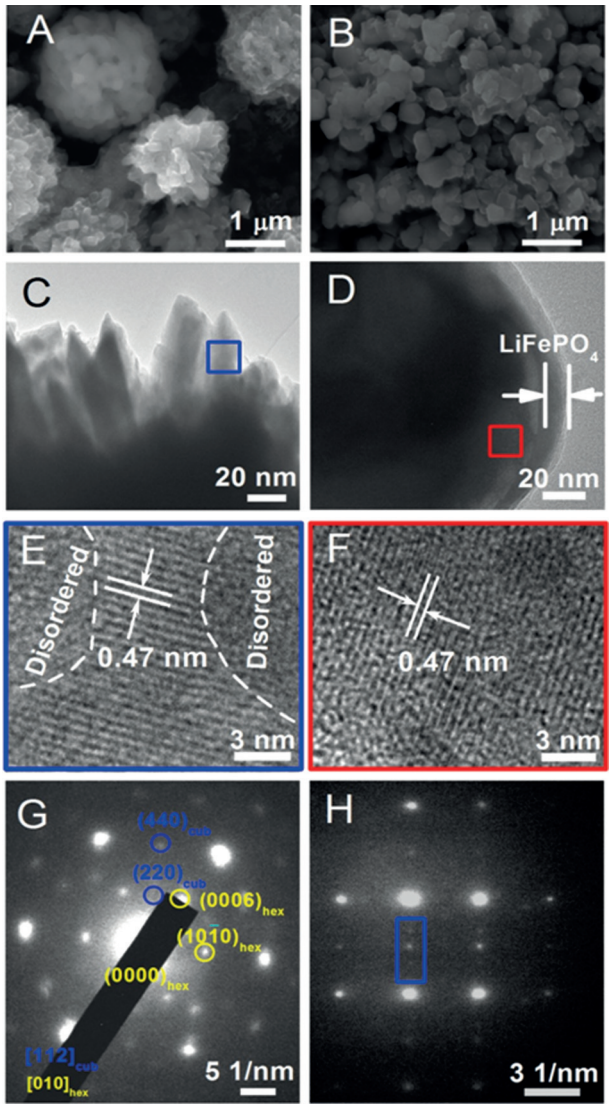

Figure 4. SEM, TEM, and HRTEM images and SEAD patterns of LLMO (A, C, E, and G) and LLMO–LFP5 (B, D, F, and H) cathode materials after 120 cycles.

Acknowledgements

We gratefully acknowledge financial support from the Natural Science Foundation of China (51402109), the Natural Science Foundation of Guangdong Province, China (S2013010014883), and the Fundamental Research Funds for Central Universities, China (2015ZZ039).

Keywords: doping · electrochemistry · lithium-ion batteries · lithium oxides · surface coatings

How to cite: *Angew. Chem. Int. Ed.* **2015**, *54*, 13058–13062
Angew. Chem. **2015**, *127*, 13250–13254

[1] J. M. Tarascon, M. Armand, *Nature* **2001**, *414*, 359–367.
[2] J. B. Goodenough, Y. Kim, *Chem. Mater.* **2010**, *22*, 587–603.
[3] J. Lu, C. Zhan, T. P. Wu, J. G. Wen, Y. Lei, A. J. Kropf, H. M. Wu, D. J. Miller, J. W. Elam, Y. K. Sun, X. P. Qiu, K. Amine, *Nat. Commun.* **2014**, *5*, 5693.
[4] F. F. Yang, Y. J. Liu, S. K. Martha, Z. Y. Wu, J. C. Andrews, G. E. Ice, P. Pianetta, J. Nanda, *Nano Lett.* **2014**, *14*, 4334–4341.
[5] B. Xu, C. R. Fell, M. F. Chi, Y. S. Meng, *Energy Environ. Sci.* **2011**, *4*, 2223–2233.
[6] A. Vu, L. K. Walker, J. Bareño, A. K. Burrell, I. Bloom, *J. Power Sources* **2015**, *280*, 155–158.
[7] I. Bloom, L. Trahey, A. Abouimrane, I. Belharouak, X. F. Zhang, Q. L. Wu, W. Q. Lu, D. P. Abraham, M. Bettge, J. W. Elam, X. B. Meng, A. K. Burrell, C. M. Ban, R. Tenent, J. Nanda, N. Dudney, *J. Power Sources* **2014**, *249*, 509–514.
[8] K. G. Gallagher, J. R. Croy, M. Balasubramanian, M. Bettge, D. P. Abraham, A. K. Burrell, M. M. Thackeray, *Electrochem. Commun.* **2013**, *33*, 96–98.
[9] J. M. Zheng, M. Gu, J. Xiao, P. J. Zuo, C. M. Wang, J. G. Zhang, *Nano Lett.* **2013**, *13*, 3824–3830.

[10] C. H. Shen, Q. Wang, F. Fu, L. Huang, Z. Lin, S. Y. Shen, H. Su, X. M. Zheng, B. B. Xu, J. T. Li, S. G. Sun, *ACS Appl. Mater. Interfaces* **2014**, *6*, 5516 – 5524.
[11] M. Gu, I. Belharouak, J. M. Zheng, H. M. Wu, J. Xiao, A. Genc, K. Amine, S. Thevuthasan, D. R. Baer, J. G. Zhang, N. D. Browning, J. Liu, C. M. Wang, *ACS Nano* **2013**, *7*, 760 – 767.
[12] S. H. Park, Y. K. Sun, *J. Power Sources* **2003**, *119*, 161 – 165.
[13] V. Subramanian, G. T. K. Fey, *Solid State Ionics* **2002**, *148*, 351 – 358.
[14] G. T. K. Fey, J. G. Chen, V. Subramanian, T. Osaka, *J. Power Sources* **2002**, *112*, 384 – 394.
[15] C. W. Park, S. H. Kim, K. S. Nahm, H. T. Chung, Y. S. Lee, J. H. Lee, S. Boo, J. Kim, *J. Alloys Compd.* **2008**, *449*, 343 – 348.
[16] S. F. Kang, H. F. Qin, Y. Fang, X. Li, Y. G. Wang, *Electrochim. Acta* **2014**, *144*, 22 – 30.
[17] G. H. Kim, S. T. Myung, H. S. Kim, Y. K. Sun, *Electrochim. Acta* **2006**, *51*, 2447 – 2453.
[18] Y. K. Sun, M. J. Lee, C. S. Yoon, J. Hassoun, K. Amine, B. Scrosati, *Adv. Mater.* **2012**, *24*, 1192 – 1196.
[19] Y. Wu, A. Manthiram, *Electrochem. Solid-State Lett.* **2006**, *9*, A221 – A224.
[20] E. Han, Y. P. Li, L. Z. Zhu, L. Zhao, *Solid State Ionics* **2014**, *255*, 113 – 119.
[21] J. Q. Zhao, Y. Wang, *Nano Energy* **2013**, *2*, 882 – 889.
[22] B. Qiu, J. Wang, Z. P. Liu, *ACS Appl. Mater. Interfaces* **2014**, *6*, 9185 – 9193.
[23] Y. J. Shi, C. W. Yi, K. J. Kim, *J. Power Sources* **2010**, *195*, 6860 – 6866.
[24] Q. Y. Wang, J. Liu, A. V. Murugan, A. Manthiram, *J. Mater. Chem.* **2009**, *19*, 4965 – 4972.
[25] S. K. Martha, J. Nanda, Y. Kim, R. R. Unocic, S. Pannala, N. J. Dudney, *J. Mater. Chem. A* **2013**, *1*, 5587 – 5595.
[26] X. Jiang, Z. H. Wang, D. Rooney, X. X. Zhang, J. Feng, J. S. Qiao, W. Sun, K. N. Sun, *Electrochim. Acta* **2015**, *160*, 131 – 138.
[27] W. Yuan, H. Z. Zhang, Q. Liu, G. R. Li, X. P. Gao, *Electrochim. Acta* **2014**, *135*, 199 – 207.
[28] S. Hy, F. Felix, J. Rick, W. N. Su, B. J. Hwang, *J. Am. Chem. Soc.* **2014**, *136*, 999 – 1007.
[29] N. Yabuuchi, K. Yoshii, S. T. Myung, I. Nakai, S. Komaba, *J. Am. Chem. Soc.* **2011**, *133*, 4404 – 4419.
[30] G. F. Xu, J. L. Li, Q. R. Xue, X. P. Ren, G. Yan, X. D. Wang, F. Y. Kang, *J. Power Sources* **2014**, *248*, 894 – 899.
[31] H. Z. Zhang, Q. Q. Qiao, G. R. Li, X. P. Gao, *J. Mater. Chem. A* **2014**, *2*, 7454 – 7460.
[32] F. H. Zheng, C. H. Yang, X. Ji, D. L. Hu, Y. Chen, M. L. Liu, *J. Power Sources* **2015**, *288*, 337 – 344.

Received: July 14, 2015
Revised: August 11, 2015
Published online: September 3, 2015

